Structures 63 (2024) 106414

Contents lists available at ScienceDirect

Structures

journal homepage: www.elsevier.com/locate/structures

General translation of cellular to shellular polyhedral structures using reciprocity

Mostafa Akbari [a], Masoud Akbarzadeh [a,b,*]

[a] Polyhedral Structures Laboratory, Department of Architecture, Weitzman School of Design, University of Pennsylvania, Philadelphia, PA, 19146, USA
[b] General Robotic, Automation, Sensing and Perception (GRASP) Lab, School of Engineering and Applied Science, University of Pennsylvania, PA, 19146, USA

ARTICLE INFO

Keywords:
Polyhedral graphic statics
Reciprocal polyhedral diagrams
Shellular structures
Compression-only
Labyrinths
Structural design
Cell-to-shell translation

ABSTRACT

Shell-based cellular (shellular) funicular structures (SFSs) are single-layer 2-manifold efficient structures with anticlastic curvature, designed in the context of graphic statics. This research proposes a comprehensive methodology for designing these efficient structures in the context of graphic statics. Due to the significant challenges in the process of designing these structures, and the ease of using 3D graphic statics in designing cellular funicular structures, this article proposes a general technique to translate any cellular funicular structure (CFS) to a shellular version (SFS). To address this transition, this study presents an integrated methodology coupled with a computational algorithm. This technique proposes a new tetrahedralization method using the reciprocal relationship between the force and the form diagrams, generalizing the translation technique. As a result, the research explores a spectrum of shellular funicular structures, under pure compression or tension states. Diverse design techniques are introduced, enabling the creation and manipulation of these structures through their three-dimensional spatial connectivity graphs, termed "labyrinths". A comparison between the structural performance of cellular and shellular funicular structures with similar volume density is performed displaying that for the same boundary condition, a shellular specimen can tolerate forces three times more than a cellular structure. To emphasize the practical utility of this design methodology, the study delves into its application at micro and meso scales. Specifically, it showcases the utilization of the shellular technique in the design of the midsole structure of a sneaker. This innovative approach draws inspiration from the pressure patterns exerted by the soles of the feet, emphasizing the adaptability and versatility of the proposed design technique. The results display that shellular funicular structures, with their lightweight and efficient nature, demonstrate superior structural capacity compared to their cellular counterparts and are applicable across micro, meso, and macro scales.

1. Introduction

1.1. Shellular structures

Shell structures are thin, curved plate structures that transfer forces through compression, tension, and shear stresses that act within the surface plane. These structures have numerous applications in science, design, and construction [1–3]. As a category of cellular structures, shell cellular (shellular) structures consist of continuous, smooth-curved shells. The geometry of these structures involves a surface with minimal material, known as a minimal surface [4]. The geometry of these surfaces, found in nature such as soap films, has inspired architects and engineers to design lightweight structures [5]. At each point on the minimal surface geometry, the mean curvature ($H = k_1 \times k_2$) is zero, and the Gaussian curvature ($G = k_1 \times k_2 < 0$, considering k_1 and k_2 as the principal curvatures of the surface) is negative [6]. Due to their high surface-to-volume ratio and unique morphology, shells with these geometries exhibit superior mechanical performance compared to other cellular structures, such as strut-based cellular structures [7–9].

1.2. Graphic statics

Graphic statics is a geometrical form-finding technique for designing structures in equilibrium for a specific boundary condition. Using this technique as an intuitive structural design method, one can design a structure using reciprocal diagrams, while controlling the internal flow of force and the external loading scenario [10–14].

Three-dimensional graphic statics (3DGS) or polyhedral graphic statics (PGS), as an extension of two-dimensional graphic statics (2DGS),

* Corresponding author at: Polyhedral Structures Laboratory, Department of Architecture, Weitzman School of Design, University of Pennsylvania, Philadelphia, PA, 19146, USA.

E-mail addresses: akbariae@upenn.edu (M. Akbari), masouda@upenn.edu (M. Akbarzadeh).

https://doi.org/10.1016/j.istruc.2024.106414
Received 2 September 2023; Received in revised form 2 April 2024; Accepted 12 April 2024
Available online 29 April 2024

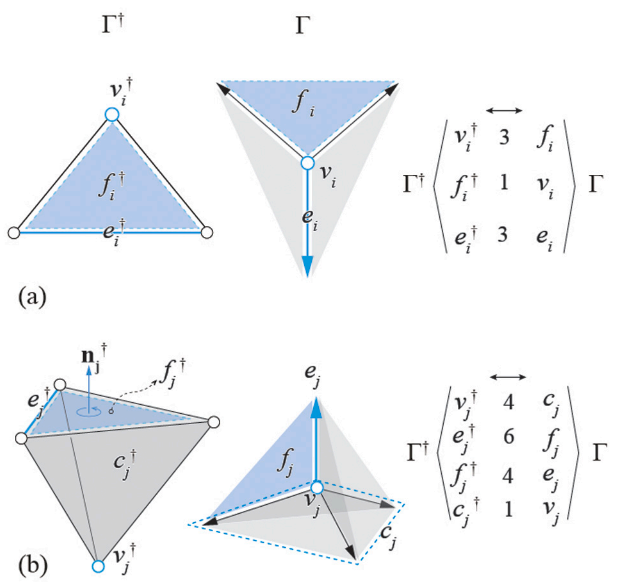

Fig. 1. Reciprocal relations between the diagrams of force (left) and form (right) in 2D graphic statics (a), and 3D graphic statics (b).

enables the user to design axially-loaded structures in 3D in which no bending occurs [15–18]. A clear relation between the *form* and *force* diagrams enables the designer to represent the equilibrium of a 3-dimensional node (form diagram) using a closed polyhedron (force diagram) (Fig. 1a). In this method, each edge e_i or force f_i in the form diagram is perpendicular to the corresponding face $f_i^{\dagger}$ in the force diagram. The form diagram represents the geometry of the structure combined with the reaction forces and applied loads, while the force diagram represents the equilibrium of internal and external forces [15]. In this paper, the form diagram is denoted by Γ and the force diagram by $\Gamma^{\dagger}$. Moreover, the force diagram's topological elements are denoted by † superscript (Fig. 1). These diagrams consist of vertices v_i, edges e_i, faces f_i, and cells c_i. Each vertex, edge, face, and cell ($v_i^{\dagger}, e_i^{\dagger}, f_i^{\dagger}, c_i^{\dagger}$) in the force diagram corresponds to a cell, face, edge, and vertex (v_i, e_i, f_i, c_i) in the form diagram [15]. In these structures, the magnitude of the force in each strut member (f_i) in the form diagram is proportional to the area of the corresponding face in the force diagram (A_{f_i}). In this technique, by applying different subdivisions to a force diagram, one is able to design various cellular strut-based structures in equilibrium. Adding thickness to each edge of the form diagram proportional to the area of its corresponding face results in a strut-based cellular funicular structure (CFS) [19].

1.3. Shellular structures in the context of graphic statics (shellular funicular structures)

Within the realm of 3D graphic statics, increasing the number of subdivisions in the force diagram yields a form diagram characterized by smaller edges and distributed forces among the members (depicted in Fig. 2a–h). This progression results in edges that approach negligible lengths, effectively approximating a surface as a form diagram. In the realm of polyhedral graphic statics, particular subdivision methodologies come into play to approximate surfaces characterized by anticlastic or synclastic curvatures as form diagrams [9].

Fig. 2a showcases a tetrahedron employed as a force diagram, corresponding to a node in equilibrium with dual upward and downward forces. This configuration represents a form diagram depicting a node with anticlastic curvature. To generate this tetrahedron, the endpoints of two skew lines, denoted as $l_i^{\dagger}$ and $l_i'^{\dagger}$, are connected. A division of these lines into equal segments, followed by establishing a tetrahedron

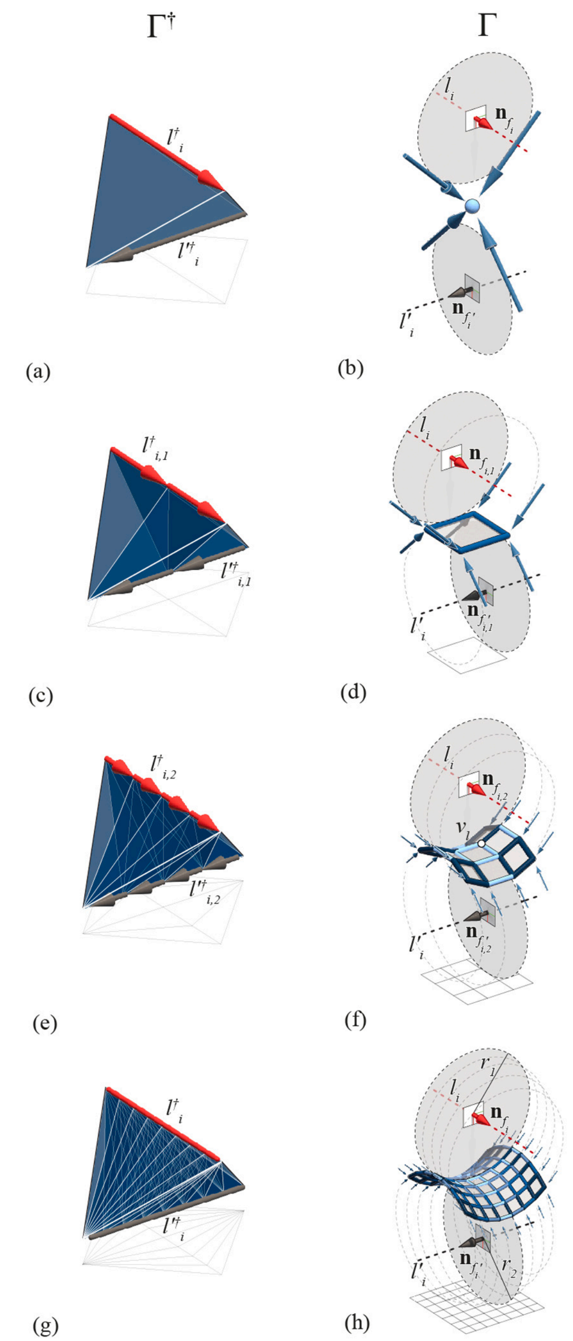

$k_1 = 1/r_1 > 0$ $k_2 = 1/r_2 < 0$ $G = k_1 \times k_2 < 0$

Fig. 2. The process of applying an anticlastic subdivision to a pair of edges (labyrinths) in the force diagram, corresponding to a discrete anticlastic surface as a form diagram.

between every pair of segments from each line, leads to the subdivision of the force diagram into multiple tetrahedrons. This process ultimately results in a discrete anticlastic surface showcased as a form diagram (as presented in Fig. 2a–d) [9,23]. Table 1 lists the nomenclatures used to describe both the introduction and the methodology section of this paper.

This specific mode of subdivision is referred to as the *anticlastic subdivision* and this group of structures are called shell-based cellular (shellular) funicular structures. These structures are efficient lightweight structures with applications in different scales, from micro-scale to macro-scale (Fig. 3) [20–22].

Fig. 3. Various applications of shellular funicular structures in the industry from microscale (a, thriply periodic shellular funicular materials [20]), to mesoscale (b, self-healing of metal shellular structures [21]), and macroscale(c, earth-based shellular structure [22]).

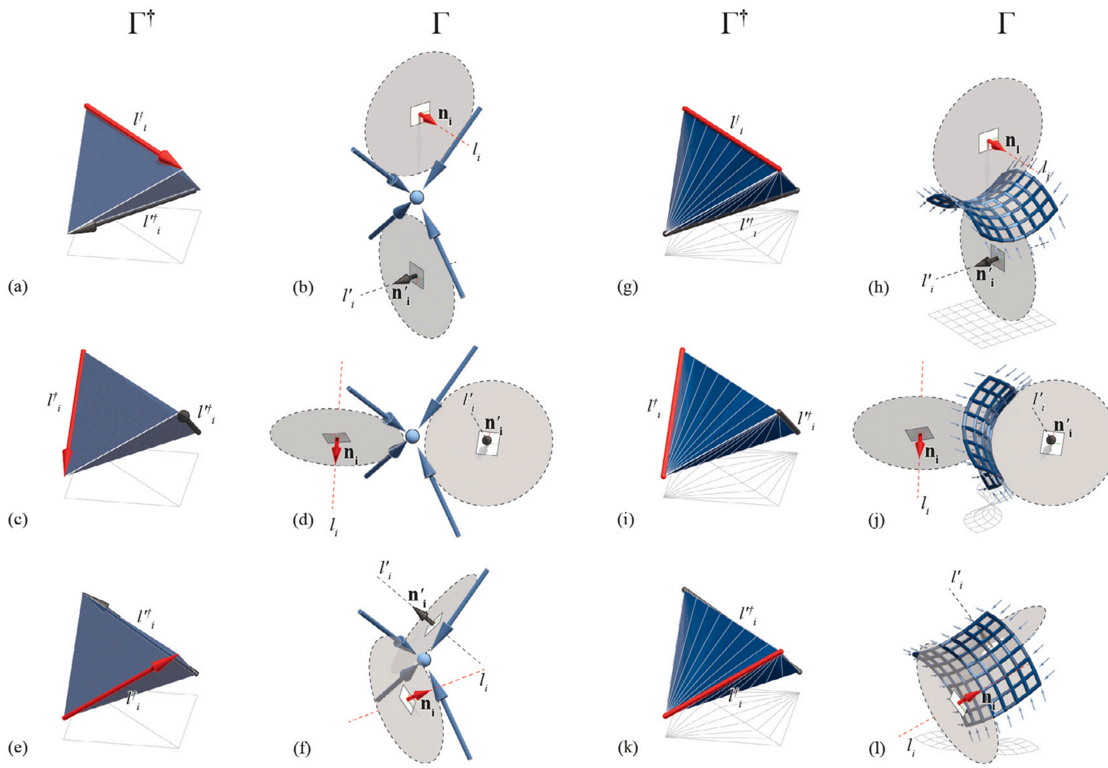

Fig. 4. Three different possibilities for designing a shell as a form diagram corresponding to a tetrahedron as a force diagram, three pairs of skew edges in a force diagram (a–f) and dividing the force diagram based on these edges results in three different shells with curvatures in different directions (g–l).

In this technique, the lines $l_i^\dagger$ and $l_i'^\dagger$ serve a dual role: as the subdivision axes within the force diagram and the curvature axes within the form diagram (as demonstrated in Fig. 2d). These lines represent components of two distinct connectivity graphs known as *labyrinths*, which link two separate regions segregated by the intervening anticlastic surface [24]. Through the utilization of the *anticlastic subdivision* technique, the design of an anticlastic polyhedral surface, denoted as a Shellular Funicular Structure (SFS), becomes achievable [20]. The labyrinths, functioning as the subdivision axes within the form and the control elements within the force, streamline the process of designing and manipulating the SFS's form-finding methodology [23]. It is worth mentioning that in this paper, all of the specimens are designed using a plugin for Rhinoceros, named Polyframe [25].

1.4. The role of labyrinths in designing and controlling the geometry of shellular funicular structures

The anticlastic surface geometry depicted in Fig. 2d effectively partitions the 3D space into two distinct subspaces, denoted as the upper and lower regions, which are determined by the shell's geometric structure. These subspaces are further characterized by their respective curvature axes, namely l_i and l_i'. In essence, these axes can be symbolic of the connectivity graph within intricate shellular geometries, often referred to as *labyrinths* [26,27]. Throughout this paper, these labyrinths are highlighted in red and black hues, exemplified in Fig. 2.

Within anticlastic geometries, the labyrinths assume the form of two interwoven graphs, with their edges consistently positioned in a *skew* orientation to each other. As the anticlastic surface resides in between, the two labyrinths become mutually intertwined, as visualized in Fig. 2d. Notably, changing the angle of these labyrinths induces modifications in the geometry of the surface [26]. It is worth mentioning that the relationship between the labyrinths in the form and force diagrams of Polyhedral Graphic Statics (PGS) (as shown in Fig. 2) is as follows: (a) the labyrinth l_i within the form diagram aligns parallel to the $l_i^\dagger$ in the force diagram; and (b) the labyrinth l_i operates as the curvature axis in the form diagram, while its counterpart in the force diagram serves as the axis for subdivision. The topology of an anticlastic surface can be comprehensively explained through its associated labyrinths [26]. In essence, adhering to the geometry and topology of prescribed labyrinths, a force diagram can be subdivided, facilitating the construction of a reciprocal compression-only or tension-only anticlastic shell, tailored to a specific loading

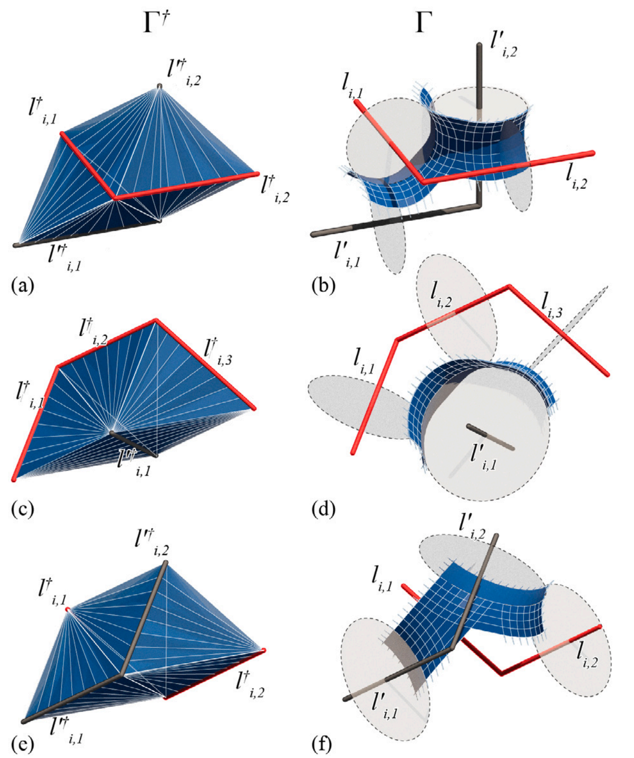

Fig. 5. Aggregation of tetrahedrons as force diagrams and subdividing them along the labyrinths (a, c, e) resulting in three different shellular geometries (b, d, f).

condition. These advancements can be accomplished by employing the methodologies inherent in PGS.

1.4.1. The labyrinths design principles

In the design process of designing shellular structures in the context of graphic statics using labyrinth graphs, certain geometrical and topological requirements should be satisfied. These requirements define the labyrinths' design principles and are as follows.

1. *Tetrahedralization* Each pair of labyrinths' edges in the force diagram should only form a tetrahedron in between, corresponding to a node with an anticlastic curvature in the form diagram (Fig. 2).
2. *Skew labyrinths* Each force diagram corresponding to a shellular architecture contains two labyrinths, including one labyrinth edge from each set. Each tetrahedron in the force diagram only includes one labyrinth edge from each set in a skew position to the other.
3. *Labyrinths' continuity* In a subdivided force diagram, each labyrinth edge in a tetrahedron can only be connected to the labyrinth' edges from the same set in the neighboring tetrahedral cell (Fig. 5).

1.4.2. Three different shellular possibilities

As mentioned in Section 1.4.1, the labyrinth graphs are in a skew position to each other in a tetrahedron and never touch each other. In each tetrahedron, there are three different possibilities for choosing these skew edges. In fact, each tetrahedron consists of 6 edges or 3 pairs of skew edges (Fig. 4a). Subdividing the force diagram based on each pair results in an anticlastic patch in a different direction (Fig. 4b). Aggregating the tetrahedrons results in shellular structures with more complexity. In fact, while aggregating the tetrahedrons, by choosing a pair of edges as the labyrinth graphs of the first tetrahedron, the labyrinth edges of the neighbor tetrahedron can be determined as well. Fig. 5 displays three different possibilities for designing shellular structures from aggregating three tetrahedrons as a force diagram. In this process, after generating the first tetrahedron (e.g., $c_i^\dagger$) and selecting the labyrinths of this tetrahedron (e.g., $l_{i,1}^\dagger$ and $l'^{\dagger}_{i,1}$), the common labyrinth $l_{i,1}^\dagger$ between this cell and its neighbor (e.g., $c_j^\dagger$), will be selected and its pair $l'^{\dagger}_{i,2}$ in the second cell will be selected. Similarly, the labyrinths of the third cell will be identified. Finally, each force diagram will be subdivided based on its labyrinths (Section 1.3), generating three different shellular structures [28].

By employing the aggregation method explained above, it becomes feasible to synthesize a shellular structure through the assembly of diverse tetrahedrons. However, this process is inherently intricate, and establishing precise boundary conditions for the structure presents a considerable challenge. In contrast, designing a strut-based cellular structure in the context of graphic statics is a straightforward process. In this process, after defining the external boundary condition of the structure, a force diagram corresponding to the boundary will be designed and it will be subdivided in order to generate a cellular structure [15]. Therefore, designing a shellular structure can start with designing a cellular structure and translating it to a shellular one. According to the principles mentioned in Section 1.4.1, each force diagram for a shellular structure should only include tetrahedrons resulting in 4-valency nodes in the form diagram (nodes that are connected to 4 edges). Although there are multiple techniques to tetrahedralize a convex polyhedron (to subdivide it into a group of non-overlapping tetrahedra) [20,28,29], one needs to ensure that identifying the labyrinths graphs in the force diagram is possible, without any geometric frustration.

1.5. Objectives and contributions

As mentioned before, strut-based cellular funicular structures comprise slender members that are prone to buckling. Furthermore, the fabrication of the nodes with complex morphologies in these types of structures is not an easy take task. In contrast, shellular funicular structures have better structural performance compared to cellular structures for the same boundary condition and volume density. The ultimate goal of this research is to create a fully automatic graphical/computational method to translate any cellular funicular structure to a shellular version. In order to achieve this goal, the labyrinth duality as a new principle will be introduced using which the force diagram of a cellular funicular structure can be translated to the force diagram of a shellular funicular structure. This translation will preserve the global force diagram, ensuring that the external boundary condition will remain the same for both cellular and the shellular version.

2. Methods

In this section, the simple process of generating an anticlastic patch in the context of graphic statics will be extended and a robust methodology for designing any shellular structure will be proposed. In this process, a robust framework is developed, translating any cellular structure to its shellular counterpart in the context of graphic statics. In the next section, a computational algorithm is introduced in order to design translate any cellular funicular structure to a shellular version. Next, different shellular forms in pure compression or tension designed for different boundary conditions will be explored. After focusing on different advantages of this technique, such as designing a hybrid shellular or cellular-shellular structures, the authors compare the structural performance of cellular and shellular architectures and explore the application of this technique in the real world. In this exploration, the mechanical properties of different shellular structures will be evaluated, and a structurally informed shellular geometry will be designed.

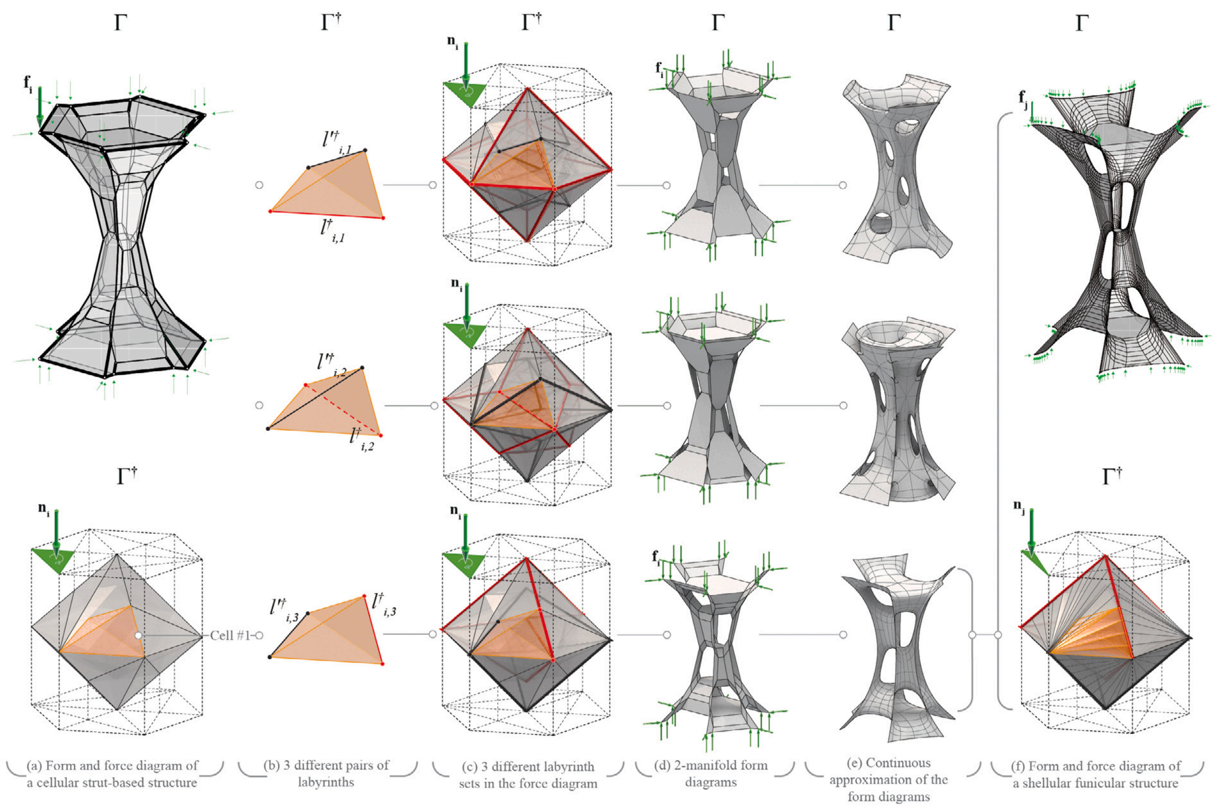

Fig. 6. An overview of the methodology that is going to be explained in the paper along with the results.

Table 1
Nomenclature for the symbols used in this paper and their corresponding descriptions.

Topology	*Description*
Γ	Form diagram (primal)
$\Gamma^\dagger$	Force diagram (dual, reciprocal)
v	# of vertices of Γ
e	# of edges of Γ
f	# of faces of Γ
c	# of cells of Γ
$v^\dagger$	# of vertices of $\Gamma^\dagger$
$e^\dagger$	# of edges of $\Gamma^\dagger$
$f^\dagger$	# of faces of $\Gamma^\dagger$
$c^\dagger$	# of cells of $\Gamma^\dagger$
$\mathbf{n}_i$	Unit normal vector of face f_i
$\mathbf{f}_i$	Point load on v_i
l_i	Edge of the labyrinth's graph in the form diagram
l'_i	Dual edge of l_i in the form diagram
$l_i^\dagger$	Edge of the labyrinth's graph in the force diagram
$l_i'^\dagger$	Dual edge of l_i in the force diagram

2.1. Results

This section describes the methodology's framework and the characteristics of the results anticipated from this approach. As depicted in Fig. 6, the methodology presented in this article facilitates the automated translation of force and form diagrams of a cellular funicular structure (Fig. 6a) into corresponding force and form diagrams of a shellular funicular structure (Fig. 6f). It is noteworthy that during this process, three distinct possibilities for labyrinth graphs exist (Fig. 6b, c), leading to the creation of three distinct two-manifold shellular structures (Fig. 6d). Furthermore, Fig. 6e visually represents the refined versions of the designed two-manifold shellular structures using the Catmull–Clark algorithm [30]. Moreover, Fig. 6f illustrates the refined version employing anticlastic subdivision within the context of graphic statics. The discrepancy between these two techniques lies in the structural force paths. Precisely, the subdivision accomplished in the context of graphic statics faithfully exhibits the exact force distribution within the structure under specific loading conditions, whereas the visualization models utilizing the Catmull–Clark algorithm merely approximate the smoothed version of the shellular structures. Previous researches emphasize that the utilization of anticlastic subdivision within the domain of graphic statics yields a geometry that is more structurally reliable, while geometries generated through the Catmull–Clark algorithm are better suited for visualization purposes [31].

2.2. Duality between the labyrinth graphs

Consider a polyhedron with its dual superimposed on top of it (Fig. 7). In order to construct the dual, it is enough to connect the center of each face to the center of the polyhedron. If we consider the edges of the polyhedron as a labyrinth graph, we realize that its labyrinth pair is the dual of the polyhedron. In fact, these graphs conform to all of the labyrinth's design principles. Each edge of one labyrinth graph (e.g., $e_{16}^\dagger$) is in a skewed position to the corresponding edges in the second graph (e.g., $e_1^\dagger$, $e_5^\dagger$, $e_8^\dagger$, $e_9^\dagger$). Therefore, one is able to construct a tetrahedron between each pair (e.g., a tetrahedron between $e_{16}^\dagger$ and $e_1^\dagger$, $e_{16}^\dagger$ and $e_5^\dagger$, $e_{16}^\dagger$ and $e_8^\dagger$, $e_{16}^\dagger$ and $e_9^\dagger$), and translate the global polyhedron to a group of non-overlapping tetrahedrons (i.e., by repeating this process to all of the edges of the black labyrinth graph). Furthermore, in each of these tetrahedrons, only one labyrinth edge from each set exists and all of the labyrinth edges from the same set are connected together.

Therefore, similar to the form and force diagrams, two labyrinth graphs are dual of each other and in a reciprocal relation. In fact, each vertex $v_i^\dagger$, edge $e_i^\dagger$, face $f_i^\dagger$, and cell $c_i^\dagger$ in the first labyrinth's graph (Fig. 7) corresponds to a cell $c'^\dagger_i$, face $f'^\dagger_i$, edge $e'^\dagger_i$, and vertex $v'^\dagger_i$ in the second set. In these labyrinths' graphs, each edge in one set (e.g., $e_1^\dagger$ in labyrinths two that are marked with red color) are in a specific angle with each face in the second labyrinth graph (e.g., $f_1^\dagger$ in labyrinth 1

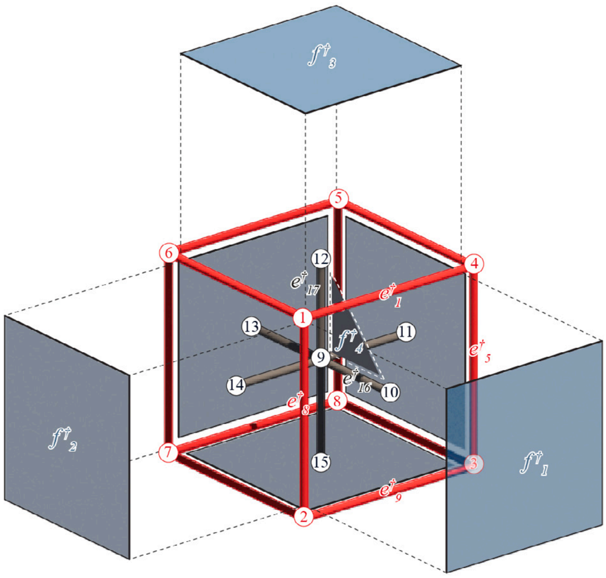

Fig. 7. Reciprocal relation between two sets of labyrinths in the context of 3D graphic statics, along with highlighting each labyrinth edge and its dual edges.

that is marked with black color). Hence, each edge of the first labyrinth graph is always in a skew position with the edges of the corresponding face in the second labyrinth graph (Fig. 7). In fact this also shows that in order to find the corresponding edges for each labyrinth edge, it is enough to find the edges of the corresponding face to that edge. Thus, by superimposing each polyhedron and its dual, one can design a pair of labyrinth graphs. Considering the polyhedron as a force diagram and its dual as a form diagram, we conclude that by superimposing each form diagram on top of the force diagram, one can generate a pair of labyrinth graphs. In this situation, each vertex in the form is inside each cell in the force and each edge in the form is in a specific angle with each face in the force diagram.

2.2.1. Tetrahedralizing the force diagram based on its dual

In this section, a general methodology is explained for tetrahedralizing a polyhedron, yielding a force diagram that allows for the identification of labyrinths and their translation into a shellular structure. This process takes advantage of the dual relationship between the force and the form diagram. According to the discussion in Section 2.2, by superimposing a polyhedron and its dual, one can result in a pair of labyrinth graphs, in which the edges of the polyhedron correspond to one graph and the edges of the dual correspond to the second graph. Therefore, by generating a tetrahedron between each edge in the first labyrinth graph and the corresponding edges in the second set, one is able to subdivide the initial polyhedron to a group of non-overlapping tetrahedrons.

Consider a tetrahedron with four faces as a force diagram corresponding to a node in equilibrium with four forces as a form diagram. A simple way to tetrahedralize this polyhedron is to superimpose its dual on top of it, generate the labyrinth graphs from the edges of the polyhedron and its dual, and tetrahedralize the polyhedron based on the labyrinths' design principles (Fig. 8a). As mentioned in Section 1.3, applying an anticlastic subdivision in each tetrahedron in a tetrahedralized force diagram between two labyrinth edges translates the force diagram to the force diagram of a shellular funicular structure (Fig. 8a). This is a general rule and can be applied to any convex polyhedron (Fig. 8c,e). Observing the generated shellular structures, we realize that all of them represent the volumetric or piped version of the internal labyrinth that is marked with black color. Applying the same process to any convex polyhedron as a force diagram results in a

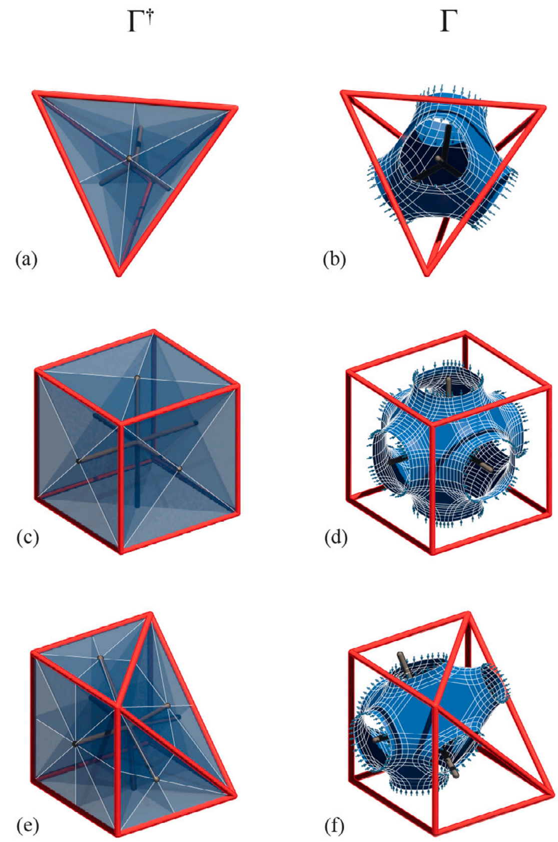

Fig. 8. Superimposing the dual of any convex polyhedron on top of that and tetrahedralizing the polyhedron based on that results in a force diagram that after applying an anticlastic subdivision (a, c, e) results in a shellular structure, displaying the piped version of the internal labyrinth (b, d, f).

shellular structure as a form diagram, representing the piped version of the internal labyrinth or in other words, the piped version of the dual of the initial polyhedron (Fig. 8).

As mentioned in Section 1.4.2, in a tetrahedralized force diagram, there are three different possible labyrinth designs, resulting in three different shellular structures. Therefore, if this tetrahedralization always results in one labyrinth set corresponding to a shellular structure, it is possible to design two more labyrinths graphs in the tetrahedralized force diagram resulting in three different shellular structures. Therefore this technique can be used in order to find three different labyrinth graphs for any polyhedron as a force diagram. Next section clearly describes the process of translating a force diagram into a shellular structure's force diagram corresponding to three different shellular funicular structures.

2.2.2. Designing shellular funicular structures

Fig. 9 displays the process of translating the force and form diagram of a cellular structure to a shellular version using the proposed tetrahedralization technique. The process starts with generating a force and the form diagram of a cellular structure (Fig. 9a,b). Next, by superimposing the force and the form diagrams on top of each other (Fig. 9c), the user is able to generate a new force diagram by tetrahedralizing the force diagram based on the two superimposed diagrams (Fig. 9d). Finally, using the method explained in Fig. 4, one can generate three different labyrinths graphs (Fig. 9e). Applying the anticlastic subdivision to each tetrahedron results in three different shellular structures.

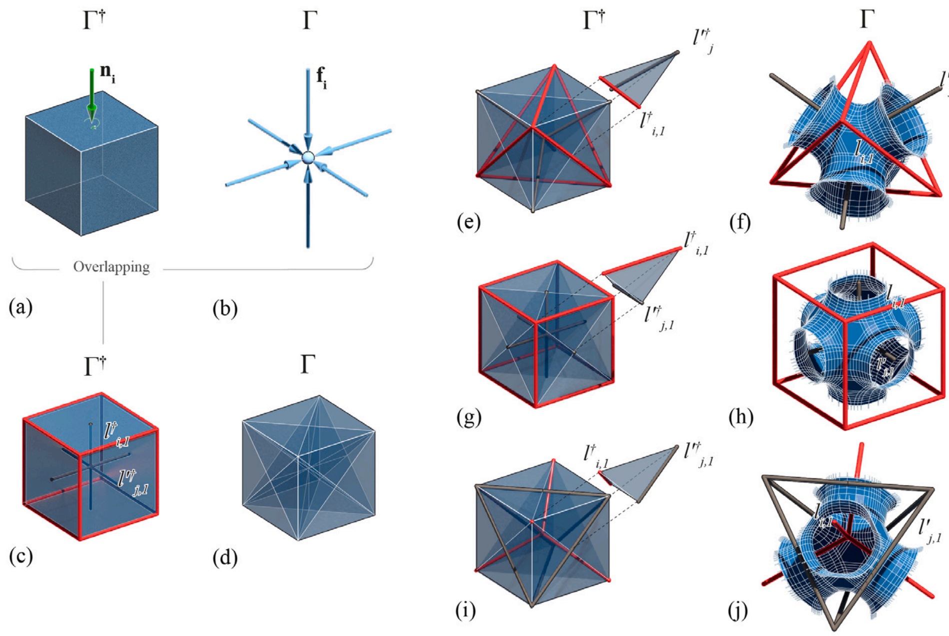

Fig. 9. Translating a cellular funicular structure to three different shellular versions by tetrahedralizing the force diagram by superimposing its dual on top of itself, (a) cellular force diagram, (b) cellular form diagram, (c) Superimposing the force and the form diagram on top of each other, (d) tetrahedralizing the polyhedron based on the superimposed diagrams, (e, g, i) generating three different labyrinth graphs in the force diagram (f, h, j) resulting in three different shellular structures.

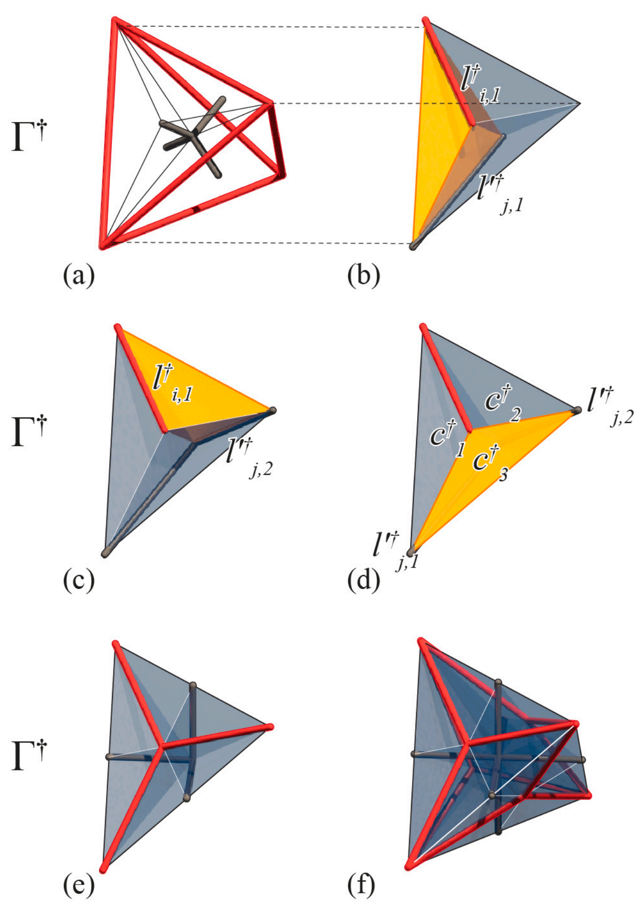

Fig. 10. Singularity in tetrahedralizing a force diagram, initial labyrinths for a tetrahedron (a), an attempt to find the second versions of the labyrinth graphs by highlighting different pairs of labyrinth edges in each cell and moving to the next cell (b,c), the highlighted cell with two labyrinth edges from the same set displaying a singularity in the process (d) and subdividing each tetrahedron cell to two cells (e) which results in resolving the singularity of the force diagram (f).

2.2.3. Singularity in translating a strut-based cellular structure to a shellular funicular structure

In order to verify the accuracy and robustness of the tetrahedralization methodology described above, it is necessary to conduct thorough testing on a variety of geometries with different topologies. In some situations, due to the specific edge-cell connectivity in a force diagram, when one edge is connected to an odd number of cells, the algorithm explained above has only one solution (instead of 3) or in more complex cases, it might not result in any solutions. Fig. 10a displays a tetrahedralized force diagram with 12 cells and possible labyrinths' graphs $l^{\dagger}_{i}$ and $l'^{\dagger}_{i}$. Figs. 10b,c,d show an attempt to find the second pair of the possible graphs. In cell $c^{\dagger}_{i,1}$, two labyrinth edges $l^{\dagger}_{i,1}$ and $l'^{\dagger}_{j,1}$ are selected. Similarly, labyrinths edges of the next cell $c^{\dagger}_{i,2}$ are $l'^{\dagger}_{i,1}$ and $l^{\dagger}_{j,2}$. Moving to the next cell $c^{\dagger}_{i,3}$, we observe that this cell includes two labyrinths $l'^{\dagger}_{j,1}$ and $l'^{\dagger}_{i,2}$ from the same set. As explained in Section 1.4.1, this situation is not acceptable according to the labyrinths' design principles. In this situation, cell $c^{\dagger}_{i,3}$ is called a singular cell. In order to solve this problem, one needs to simply divide all the cells (e.g., cell $c^{\dagger}_{i,3}$) into two cells (e.g., cells $c^{\dagger}_{i,4}$ and $c^{\dagger}_{i,5}$). Fig. 10e,f displays that in the new condition, one is able to properly design the second possible labyrinth sets. It is worth mentioning that this is a general solution for the tetrahedralization and can be repeated in any other geometry in order to design shellular structures (see Fig. 13).

2.3. Computational implementation of translating any strut-based cellular funicular structure to a shellular funicular structure

This section explains an algorithm to translate any cellular funicular structure to three different shellular funicular structures (Fig. 11). The algorithm starts with receiving a force and form diagram of a cellular funicular structure as inputs (Fig. 12a). As mentioned in Section 1.4.2, in order to generate a shellular structure, one needs to ensure that the form diagram only includes 4 valency vertices. Therefore, the force diagram should only include tetrahedrons. If the force diagram is already tetrahedralized, the algorithm moves to the next step. If not, it uses the tetrahedralization method that is explained in Section 2.2.1 to tetrahedralize the force diagram using the initial force diagram and

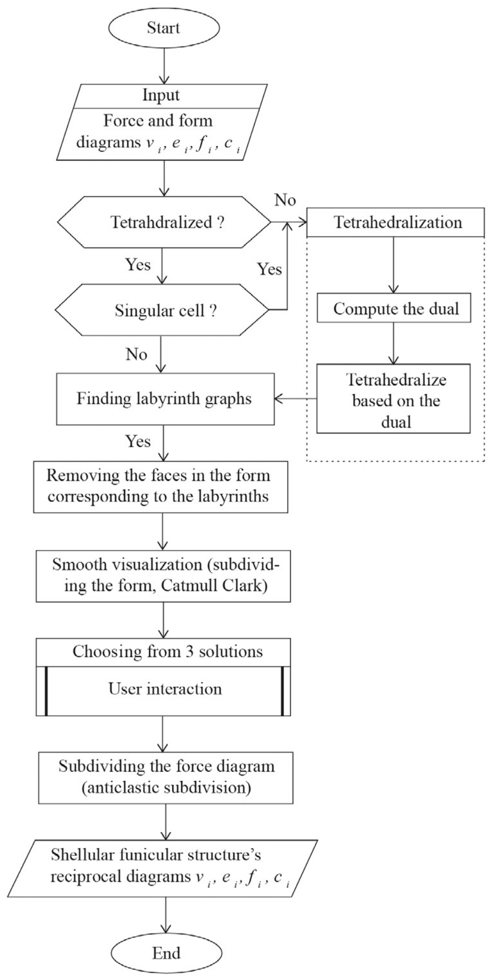

Fig. 11. The flowchart for translating any cellular funicular structure to three different shellular funicular structures.

its reciprocal form diagram. In the next stage, the algorithm iteratively searches through each cell and finds the labyrinths of the cells. In this process, if any singularity happens in the process, as explained in Fig. 10, each cell will be divided into two cells to change the edge-cell connectivity to resolve the singularity. After finding the first labyrinth graphs, using the method explained in Section 1.4.2, the algorithm finds two other possible labyrinth graphs (Fig. 12b, c). At this level, the user can visualize the force diagram in order to choose between three different shellular structures. In order to generate the shellular form diagram, the algorithm generates the form diagram by materializing the edges and then, it materializes all the faces except the ones corresponding to the labyrinth edges in the force diagram in order to result in a two-manifold solution (Fig. 12d) [28]. Afterward, the user can use any smoothing algorithm (e.g., Catmull Clark algorithm [30, 31]) to visualize the smooth version of the 2-manifold form diagram. After choosing the desired form, the algorithm applies an anticlastic subdivision to the force diagram to subdivide it along its labyrinths (Section 1.3) (Fig. 12e). Finally, by generating the form diagram of the subdivided force diagram and materializing the faces, except the ones corresponding to the labyrinth graphs, the user results in a shellular funicular form diagram (Fig. 12f) (see Fig. 14).

2.4. Exploring shellular forms in pure compression or tension

In this section, an assortment of illustrations is presented to demonstrate the application of the proposed method in the design of shellular and cellular/shellular structures. Fig. 12 displays a group of shellular funicular forms designed for different boundary conditions. The first group shows the design of three different shellular funicular column structures designed for specific boundary conditions with loads from the top and the bottom of the structure (Fig. 12a–e). The example starts with tetrahedralized force diagram representing a cellular structure (Fig. 12a). Next, a cell will be chosen as the first cell for designing the labyrinth graphs and its labyrinth edges will be marked (Fig. 12b). Afterward, in an iterative process, the labyrinth edges of the whole force diagram will be designed (Fig. 12c). After visualizing the two manifold form diagrams corresponding to the force diagram with labyrinth graphs (Fig. 12d), the smooth version of the form diagrams will be visualized in order to give the user the opportunity to choose between them (Fig. 12e). Finally, an anticlastic subdivision will be applied to the force diagram to subdivide it along with the chosen labyrinth graph, resulting in the subdivided shellular funicular form diagram (Fig. 12f). The second example displays the visualization of three different shellular possibilities for designing a dome structure (Fig. 12f–j). Similarly, the last example explores different possibilities for designing a shellular funicular bridge structure (Fig. 12k–o).

2.4.1. Constraining the boundary conditions of shellular funicular structures

When designing a structure with specified boundary conditions using 3D graphic statics, it is crucial to understand the procedure for constraining the boundary edges of the structure to a specific plane. For instance, Fig. 12a illustrates the form and force diagrams associated with a column that is constrained between two surfaces, such as the ceiling and the floor. The force diagram highlights the cells that have been added to confine the column within the two surfaces, indicated by dashed lines. To constrain the force diagram to a particular surface, it is necessary to extrude the force diagram along the constrain surface's normal vector and then intersect it with a parallel surface of choice. In this example, the force diagram is extruded upwards and downwards, and intersected with surfaces parallel to the constraining ones. In Fig. 12k–o, the dome is solely constrained to the floor. Therefore, the force diagram is extruded downwards and intersected with a surface parallel to the ground surface. In Fig. 12f–j, the bridge is constrained on both sides in the x direction and also on the top. Consequently, the force diagram is extruded in the x and z directions, and intersected with the yz and xy planes. Similarly, like the force diagram of a cellular structure, the force diagram of a shellular structure can also be confined to a specific plane. Fig. 12f demonstrates the process of constraining a shellular force diagram to planes parallel to the xy plane, situated at the top and bottom of the structure.

2.4.2. Designing hybrid cell-shell structures

This section explains the process for designing a hybrid structure ranging from cellular to shellular funicular structures. In this example, the structure that has been shown in Fig. 9f is redesigned using four different levels of subdivisions in order to visualize structures ranging from strut-based cellular to shell-based cellular (shellular) (Section 2.4.2). In order to connect the force diagrams of these structures together, due to the difference in the level of subdivision, one needs to design connection cells between the force diagrams corresponding to branching elements in the form diagram. For instance, connecting section A to B of the form diagram requires adding the branching element consisting of edges e_1, e_2, e_3, and f_1 in the form diagram, corresponding to the cell $c_1^{\dagger}$ in the force diagram. Similarly, other sections of the form diagram can be attached together, representing a hybrid cellular/shellular funicular structure designed for a defined boundary condition. In fact, this is one of the greatest benefits of this technique since it allows the user to combine different structures with various design languages while maintaining the boundary condition and equilibrium of the system.

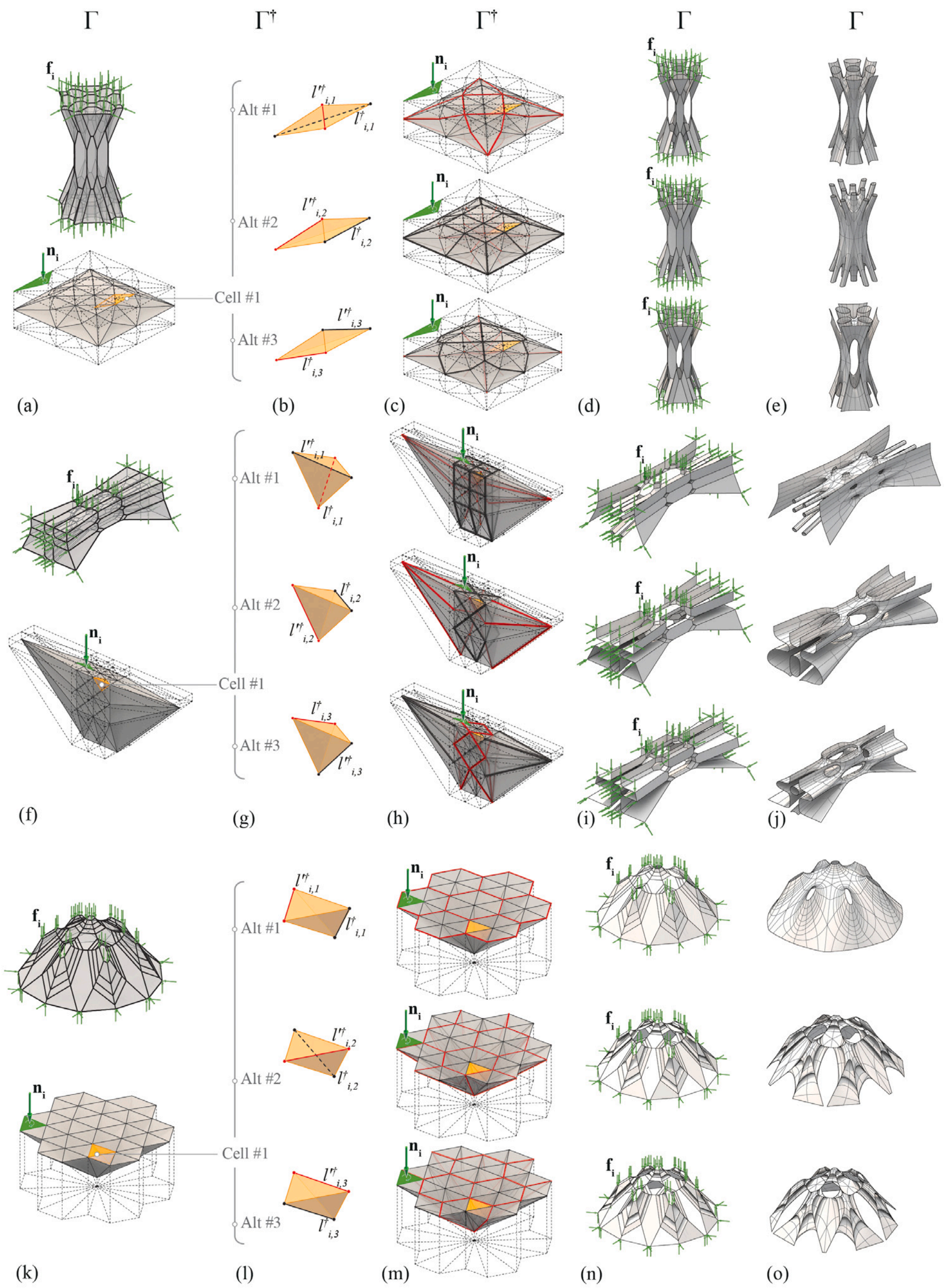

Fig. 12. Exploring shellular forms in pure compression or tension, the force and form diagrams of s cellular structure with loads from the top and the bottom of the structure approximating a column (a), selecting three different pairs of labyrinth in a cell in the force diagram (b) which results in three force diagrams with three distinct labyrinth graphs (c) corresponding to three different two manifold shellular structures before smoothing (d), and after smoothing using Catmull Clark algorithm (e). Next row (f–j) displays the same elements for a bridge and section the below section (k–o) displays the same process for a dome.

Table 2
Comparing specimens' stiffness (N/mm), surface area (mm^2), average mean curvature(1/mm), maximum mean curvature (1/mm), and yield point(N).

	Stiffness (N/mm)	Surface area (mm^2)	Average mean curvature (1/mm)	Maximum mean curvature (1/mm)	Yield point (N)
Shellular 1	93.29	7,125	0.046	0.09	300
Shellular 2	125.47	13,247	0.097	0.19	450
Shellular 3	150.10	12,098	0.210	0.43	550

2.4.3. Designing a hybrid shellular structure

Similar to the design described in the preceding section, it is possible to merge various shellular structures under specific circumstances. Fig. 15 illustrates this concept, where two shellular structures are combined by integrating their force diagrams while maintaining a consistent labyrinth design at the intersection. It is crucial to ensure that the edges of one structure align with the edges of the other structure at the connection point. Consequently, when the labyrinth design at

Fig. 13. Physical models of a group of 3D printed cellular and shellular funicular structures, in each row, the first column displays a cellular funicular structure and the rest represents three different shellular possibilities.

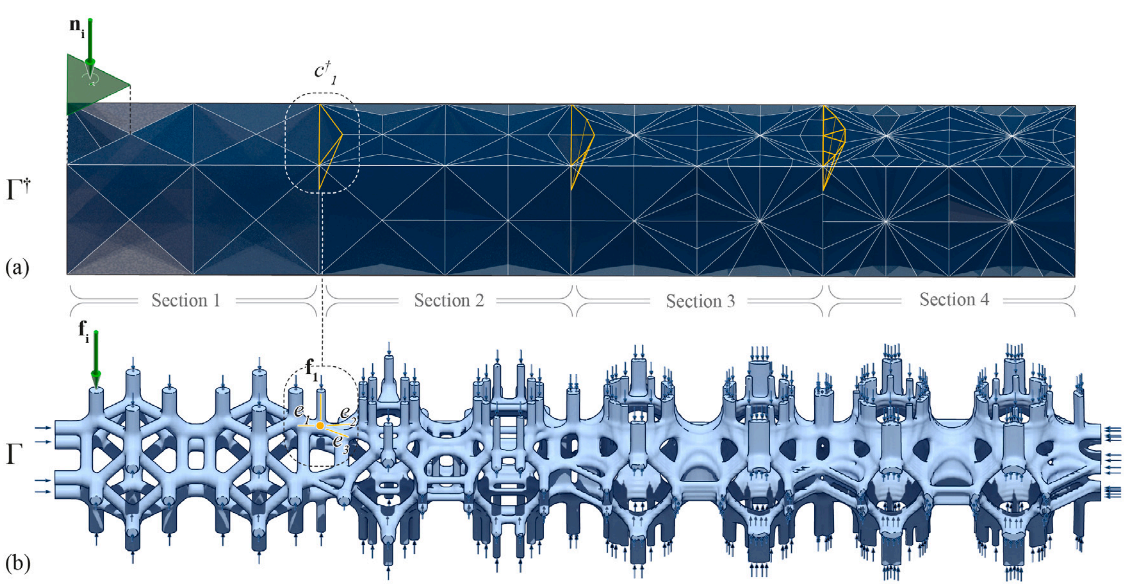

Fig. 14. Designing a hybrid cell-shell structure, the force diagram of a hybrid cell-shell structure with highlighted branching cells (a), and the form diagram of a cell-shell funicular structure highlighting the branching section, joining two sections of the structure with different number of subdivisions (b) (it is important to notice that in this form diagram, the edges have been materialized in contrast with the previous figures in which the faces in shellular form diagrams were materialized.).

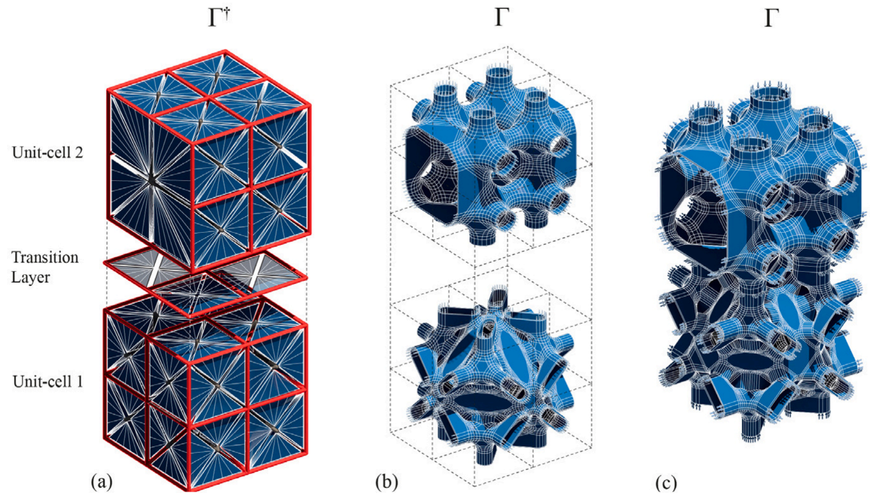

Fig. 15. Designing a hybrid shellular structure, the force diagram of a hybrid shellular structure comprising two different force diagrams with similar transition layer (a), the form diagrams of two shellular structures (b), and the form diagram of the hybrid shellular structure (c).

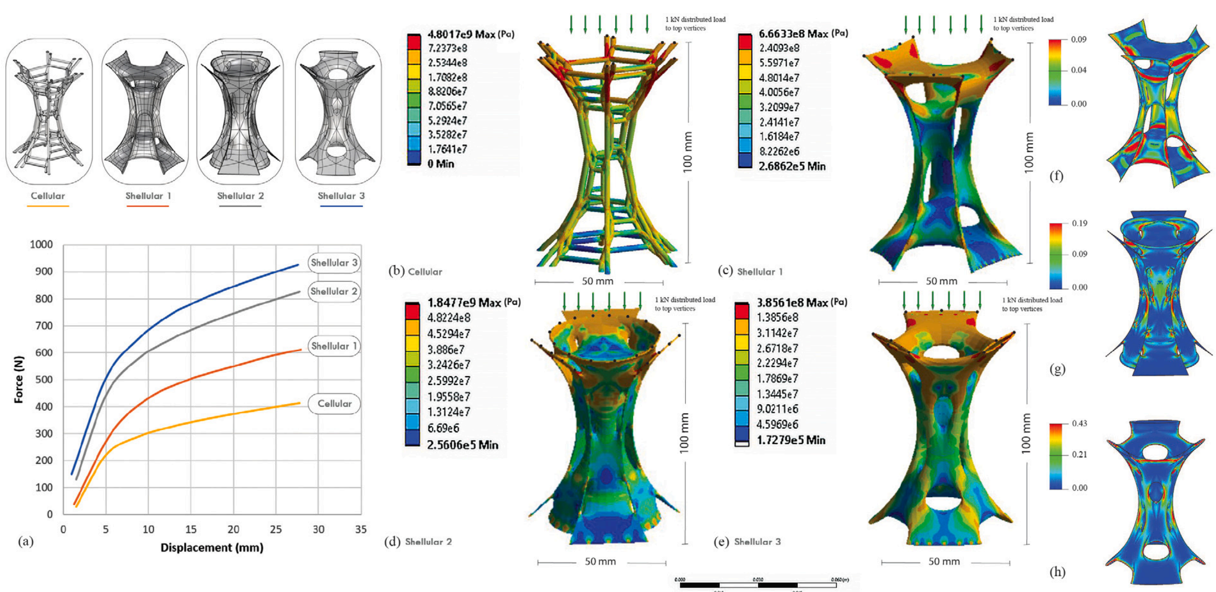

Fig. 16. Comparing the structural performances of cellular and shellular funicular structures. Load–displacement curves of cellular and shellular specimens (a) Mises stress contour of the cellular specimen (b), Mises stress contour of the shellular 1 specimen (c), shellular 2 specimen (d), and shellular 3 specimens (e) along with their mean curvature distribution heat map (f, g, h).

the boundary is identical, the force diagrams of the two structures can seamlessly merge together.

3. Results

This section concentrates on Comparing structural performances of cellular and shellular funicular structures and one of the applications of the proposed technique for designing shellular funicular structures in the industry.

3.1. Comparing structural performances of cellular and shellular funicular structures

Cellular funicular structures are characterized by slender, elongated members that are susceptible to buckling under load. Various numerical analyses demonstrate that shellular funicular structures exhibit superior structural performance in comparison to their cellular funicular counterparts [9,20]. Fig. 16 displays a numerical analysis of the structural characteristics of cellular structure and its shellular counterparts to investigate the mechanical response of distinct structures, all of them composed of steel and possessing identical relative density. In this comparison, the structures displayed in Fig. 6 have been compared to each other. Each structure's relative density ρ is defined as V_s/V_{RVE} where V_s and V_{RVE} denote the volume of the solid material in the structure and representative volume element or the volume of the bounding box, respectively. Each of these structures with a volume of 5810 mm^3 has been designed for a boundary box with a volume of $250,000$ mm^3 (50 mm × 50 mm × 100 mm). Therefore, the relative density of each structure is equal to 0.02. Each structure is simply supported from the bottom and tolerates a distributed load of 1 kN from the top along the Z axis. Employing tetrahedral meshes containing approximately half a million elements, all specimens are modeled using an elastic, perfectly plastic behavior model, subject to similar boundary conditions, loading

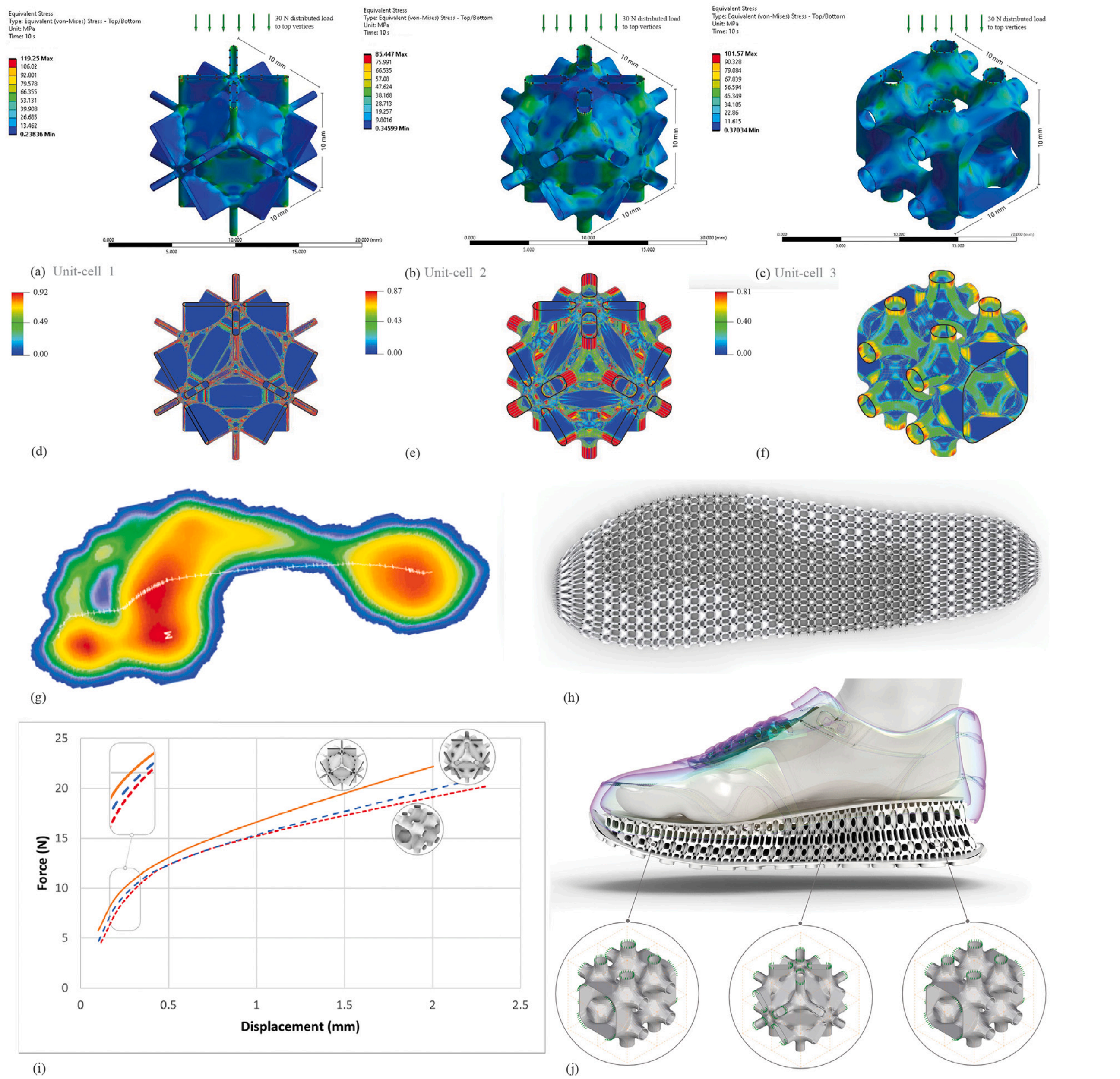

Fig. 17. Application of shellular funicular structures designed in the context of graphic statics, equivalent stress of three different shellular funicular unit-cells designed in PGS (a–c), the mean curvature distribution heat map of the unit-cells (d–f), the podometry study of a foot (g) [32] ©*Medicapteurs*, plan view of a midsole of a sneaker designed and adapted to the podometry study using shellular technique (h), the force displacement chart displaying three structures with different stiffnesses (i), and the front view of the designed sneaker's midsole along with the micro structures distributed based on the podometry study (j).

rate, and element types. The load–displacement curve shows that for a similar displacement in these specimens (e.g., 2.5 mm), the shellular specimens can tolerate higher loads than the cellular version (i.e., 150, 250, and 350 N for the shellular specimens compared to 100 *N* for the cellular version). In fact, adding faces between the struts in the shellular model results in a structure with better structural performance, specifically higher shear capacity [20]. Table 2 illustrates a comparison of stiffness, surface area, average mean curvature, maximum mean curvature, and yield point among different specimens. Upon examination, it becomes evident that shellular specimen no. 3 is stiffer than no. 2, no. 2 is stiffer than no. 1, and all these specimens exhibit greater stiffness than the cellular structure. The same pattern is observed in the yield points, average mean curvature, and maximum mean curvature. However, there is no correlation between the surface area and the stiffness of the structure. Clearly, further investigation is required to establish a connection between the curvature of the structure and its stiffness. It is important to notice that in these comparisons, the geometry of the structures before the materialization is considered. Therefore, surface area and curvature do not have a meaning for cellular structures, comprising linear elements and are only measured for the shellular structures.

3.2. Application of shellular funicular structures designed in the context of graphic statics

The field of footwear design constantly seeks to incorporate fresh concepts, advanced technology, and innovative materials in order to enhance comfort, safety, durability, performance, and quality. Through laboratory measurements, designers gain valuable insights into the impact of their designs, novel materials, and performance-enhancing

Table 3
Comparing unit-cells' stiffness (N/mm), surface area (mm^2), average mean curvature(1/mm), maximum mean curvature (1/mm), and yield point(N).

	Stiffness (N/mm)	Surface area (mm^2)	Average mean curvature (1/mm)	Maximum mean curvature (1/mm)	Yield point (N)
Unit-cell 1	34.01	380	0.49	0.92	9
Unit-cell 2	31.84	430	0.43	0.87	8
Unit-cell 3	30.48	379	0.40	0.81	7.5

features. When developing footwear, it is crucial to prioritize the creation of products that take into account the pressure endured by the feet, ensuring that the design is well-informed in this regard. This section focuses on designing structurally-informed shoes using the shellular methodology that is explained in this paper. In this process, the focus is on the design of the midsole of a shoe in order to optimize the stiffness of the midsole according to the pressure endured by the feet. To create a structurally informed midsole design, the authors concentrate on developing diverse shellular micro-structures with varying levels of stiffness tailored to different sections of the midsole.

3.2.1. Evaluating structural performance of different shellular unit-cells

The design process starts with designing different shellular funicular structures with similar relative densities. Fig. 17a–c displays the structural performance of three different shellular unit-cells designed using the proposed technique. Each of these unit-cells with a volume of 37 mm^3 has been designed for a boundary box with a volume of 3375 mm^3 (15 mm × 15 mm × 15 mm). Therefore, the relative density of each unit-cell is equal to 0.01. A numerical structural analysis is performed to study the mechanical behavior of three different shellular funicular structures shown in Fig. 17a–c, fabricated using additive manufacturing technique, made out of Polylactic Acid or PLA. A tetrahedral mesh consisting of approximately half a million elements is generated for all specimens using elastic perfectly plastic behavior with similar boundary conditions, loading speed, and type of elements. Each structure is simply supported from the bottom and is tolerating a distributed load of 30 N from the top along the Z axis. The preliminary load–displacement curve (Fig. 17i) demonstrates that the three structures exhibit distinct stiffness behaviors within the elastic regime. Different stiffness results in different flexibility, making each structure suitable for specific loading conditions. Table 3 investigates a relation between the structures' stiffness, curvature, and yield points. Similar to Table 2 Increasing the surface area and maximum curvature in a structure has resulted in a stiffer specimen. Certainly, we cannot make a broad generalization about the connection between curvature and stiffness for all shell structures. Further research is necessary to thoroughly explore this topic.

3.2.2. Designing structurally informed shoes using shellular methodology

The design process begins by analyzing the podometry diagram (Fig. 17g), which provides valuable information about the pressure distribution exerted by the foot on a surface. Subsequently, different regions of the midsole experiencing varying levels of pressure are covered with shellular structures of appropriate stiffness. Areas with higher pressure are covered with structures of lower stiffness, while areas with lower pressure are covered with structures of higher stiffness in order to properly absorb the pressure exerted by the feet. This design approach ensures that the midsole's structure is suitably flexible to interact with the feet's pressure, effectively accommodating and equalizing varying force levels. The final design of the structurally informed footwear is depicted in Figs. 17h and 17j. In this design, the unit cells are morphed along each area, with parts possessing lower stiffness acting as energy absorbers. This design feature helps to equalize the pressure experienced by the foot, enhancing overall comfort and support.

4. Conclusion

This research introduces a fully automatic graphical method that allows for the translation of any cellular funicular structure into a shellular version. This translation process ensures that the global force diagram remains preserved, guaranteeing consistency in the external boundary conditions between the cellular and shellular versions. Using this method, users have ample flexibility to manipulate and modify the design to suit different loading scenarios. Additionally, users have control over the magnitude of the forces on each edge of the shellular structure, corresponding to the areas of the faces in the force diagram. This allows for the allocation of more material to edges experiencing higher forces, effectively balancing the force distribution within the system. The tetrahedralization method that is provided in this research enables the user to translate any cellular funicular structure into a shellular funicular structure. Furthermore, for each cellular structure, the technique proposes three distinct shellular structures, providing users with the freedom to choose the most suitable option.

In the final section of the research, the structural performances of cellular and shellular funicular structures designed using this method, along with the application of the proposed technique in the design of a group of shellular micro-structures are explored, highlighting its practical implementation and potential advantages. Due to their specific geometry, cellular funicular structures' mechanical capacity depends on the buckling performance of the struts. On the flip side, shellular funicular structures exhibit superior structural performance in terms of load-bearing capacity, stiffness, and shear capacity, thanks to their specific geometries that include faces with anticlastic curvatures. One notable limitation of designing cellular structures using 3D graphic statics is the structural stability of the geometry under loading scenarios that they are not designed for. Each cellular structure, designed within the context of graphic statics, achieves equilibrium for a particular boundary condition. Consequently, the structure primarily exhibits stretching-dominated behavior only for that specific loading scenario. However, when the loading conditions change, the structure tends to behave more like a bending-dominated structure. A recent study by Akbari et al. (2022) [20] addresses this issue and highlights that shellular funicular structures, in contrast to cellular funicular structures, tend to exhibit stretching-dominated behavior even when subjected to boundary conditions they were not specifically designed for. In Section 3.2, three shellular funicular structures are designed for three different directions (x, y, and z), with the major loading occurring along the z axis. In fact that is why shellular structures are better suited for this particular application, as they can effectively handle the predominant loading direction and maintain their stretching-dominated behavior. As a result, for the same boundary condition, a shellular specimen can tolerate forces three times more than a cellular structure.

The developed methodology presents a versatile framework for the creation of novel shellular structures with hybrid topologies, allowing for tuning their mechanical properties. This framework holds significant potential for various applications, ranging from engineering tissue scaffolds at the microscale to the structure of artificial bones at the mesoscale, and even to larger-scale applications such as buildings or bridges.

However, various research aspects necessitate additional investigation. The design methodologies presented within the framework of graphic statics do not account for the structure's self-weight in force equilibrium. Additionally, this is a material-independent technique that solely addresses structural geometry. Consequently, the authors plan to shift their focus in the future towards incorporating self-weight and material characteristics into the design process, aiming to create a more comprehensive and precise design technique. Moreover, additional studies are required to examine the correlation between a structure's average curvature, maximum curvature, and stiffness. This is essential for making generalizations based on the findings presented in this article.

CRediT authorship contribution statement

Mostafa Akbari: Conceptualization, Data curation, Formal analysis, Investigation, Methodology, Validation, Visualization, Writing – original draft, Writing – review & editing. **Masoud Akbarzadeh:** Conceptualization, Funding acquisition, Methodology, Project administration, Resources, Software, Supervision, Validation, Writing – review & editing.

Declaration of competing interest

The authors declare that they have no known competing financial interests or personal relationships that could have appeared to influence the work reported in this paper.

Acknowledgments

This research was funded by the National Science Foundation CAREER Award (NSF CAREER-1944691 CMMI) and the National Science Foundation Future Eco Manufacturing Research Grant (NSF, FMRG-CMMI 2037097) to Dr. Masoud Akbarzadeh.

References

[1] Teng Teng, Jia Mian, Sabin Jenny E. The designing of epithelial cell inspired-brick inmasonry shell system. 2020, https://api.semanticscholar.org/CorpusID:222140125.
[2] Teng Teng, Sabin Jenny. The design and 4d printing of epithelial cell-inspired programmable surface geometry. CUMINCAD; 2021.
[3] Adriaenssens Sigrid, Block Philippe, Veenendaal Diederik, Williams Chris. Shell structures for architecture: form finding and optimization. Routledge; 2014.
[4] Meeks III William, Pérez Joaquín. The classical theory of minimal surfaces. Bull Amer Math Soc 2011;48(3):325–407.
[5] Burkhardt Berthold. Natural structures-the research of frei otto in natural sciences. Int J Space Struct 2016;31(1):9–15.
[6] Hilbert David, Cohn-Vossen Stephan. Geometry and the Imagination, vol. 87, American Mathematical Soc.; 2021.
[7] Han Seung Chul, Lee Jeong Woo, Kang Kiju. A new type of low density material: Shellular. Adv Mater 2015;27(37):5506–11.
[8] Han Seung Chul, Choi Jeong Myung, Liu Gang, Kang Kiju. A microscopic shell structure with Schwarz's D-surface. Sci Rep 2017;7(1):1–8.
[9] Akbari Mostafa, Akbarzadeh Masoud, Bolhassani Mohammad. From polyhedral to anticlastic funicular spatial structures. In: Proceedings of IASS symposium. 2019.
[10] Maxwell JC. On reciprocal figures and diagrams of forces. Philos Mag Series 4 1864;27(182):250–61.
[11] Rankine WJM. Principle of the equilibrium of polyhedral frames. Philos Mag Series 4 1864;27(180):92.
[12] Beghini LL, Carrion J, Beghini A, Mazurek A, Baker WF. Structural optimization using graphic statics. Struct Multidiscip Optim 2013;49(3):351–66.
[13] Cremona L. Graphical statics: Two treatises on the graphical calculus and reciprocal figures in graphical statics. Translated by Thomas Hudson Beare. Oxford: Clarendon Press; 1890.
[14] Culmann K. Die graphische statik. Zürich: Verlag Meyer und Zeller; 1864.
[15] Akbarzadeh M. 3D graphic statics using reciprocal polyhedral diagrams [Ph.D. thesis], Zurich, Switzerland: ETH Zurich; 2016.
[16] Lu Y, Cregan M, Chhadeh PA, Seyedahmadian A, Bolhassani M, Schneider J, et al. All glass, compression-dominant polyhedral bridge prototype: form-finding and fabrication. In: Proceedings of IASS symposium and spatial structures conference 2020/21, inspiring the next generation. 2021.
[17] Zheng Hao, Hablicsek Marton, Akbarzadeh Masoud. Lightweight structures and the geometric equilibrium in dragonfly wings. Int Assoc Shell Spatial Struct 2021.
[18] Zheng Hao, Wang Xinyu, Qi Zehua, Sun Shixuan, Akbarzadeh Masoud. Generating and optimizing a funicular arch floor structure. Assoc Computer-Aided Architect Des 2021.
[19] Akbarzadeh M, Tabatabaie Ghomi A, Bolhassani M, Akbari M, Seyedahmadian A, Sun J, et al. Saltatur: Node-based assembly of funicular spatial concrete. In: Proceedings of the 40th annual conference of the association for computer-aided design in architecture. 2021.
[20] Akbari Mostafa, Mirabolghasemi Armin, Bolhassani Mohammad, Akbarzadeh Abdolhamid, Akbarzadeh Masoud. Strut-based cellular to shellular funicular materials. Adv Funct Mater 2022;2109725.
[21] Hsain Zakaria, Akbari Mostafa, Prasanna Adhokshid, Jiang Zhimin, Akbarzadeh Masoud, Pikul James H. Electrochemical healing of fractured metals. Adv Mater 2023;2211242.
[22] Lasting Liam N, Isabelle Lee Isabelle, Laia Mogas-Soldevila Laia, Akbarzadeh Masoud. Terrene 1.0: Innovative, earth-based material for the construction of compression-dominant shell structures. In: Proceedings of IASS symposium and spatial structures conference 2022, innovation sustainability legacy. Beijing, China, 2022.
[23] Akbari Mostafa, Mirabolghasemi Armin, Akbarzadeh Hamid, Akbarzadeh Masoud. Geometry-based structural form-finding to design architected cellular solids. In: Symposium on computational fabrication. 2020, p. 1–11.
[24] Fischer Werner, Koch Elke. Genera of minimal balance surfaces. Acta Crystallogr Sect A 1989;45(10):726–32.
[25] Nejur Andrei, Akbarzadeh Masoud. PolyFrame, efficient computation for 3D graphic statics. Comput Aided Des 2021;134:103003.
[26] Fischer W, Koch E. Genera of minimal balance surfaces. Acta Crystallogr Sect A 1989;45(10):726–32.
[27] Fischer W, Koch E. Crystallographic aspects of minimal surfaces. Le J Phys Colloques 1990;51(C7):C7–131.
[28] Akbari M, Lu Y, Akbarzadeh M. From design to the fabrication of shellular funicular structures. In: Proceedings of the association for computer-aided design in architecture. 2021.
[29] Toussaint Godfried T, Verbrugge Clark, Wang Cao An, Zhu Binhai. Tetrahedralization of simple and non-simple polyhedra. In: CCCG. 1993, p. 24–9.
[30] Catmull Edwin, Clark James. Recursively generated B-spline surfaces on arbitrary topological meshes. Comput Aided Des 1978;10(6):350–5.
[31] Akbari M, Akbarzadeh M. Continuous approximation of shellular funicular structures. In: Proceedings of IASS 2022 symposium affiliated with APCS 2022 conference. 2022.
[32] Medicapteurs. Baropodometry. 2023, https://www.medicapteurs.com.